

Article

# Single Crystal Diamond Deposited by Dual Radio-Frequency Plasma Jet CVD with High Growth Rate

Hao Liu , Jia-jun Li, Zhen-rui Li, Kai Xu, Zheng-jia Chen and Guang-chao Chen \*

College of Materials Science and Opto-Electronic Technology, University of Chinese Academy of Sciences, Beijing 100049, China; liuhao13@mails.ucas.ac.cn (H.L.); lijiajun12@mails.ucas.ac.cn (J.-j.L.); lizhenrui16@mails.ucas.ac.cn (Z.-r.L.); xukai17@mails.ucas.ac.cn (K.X.); chenzhengjia18@mails.ucas.ac.cn (Z.-j.C.)

\* Correspondence: gcchen@mails.ucas.ac.cn

Received: 3 December 2018; Accepted: 6 January 2019; Published: 10 January 2019



**Abstract:** Single crystal diamonds were deposited on high pressure high temperature (HPHT) substrate with high growth rate, up to 18.5  $\mu\text{m}/\text{h}$ , by using dual radio-frequency inductive coupled plasma jet. The methane flux was found to influence the growth rate of single crystal diamond. The reason for this might be ascribed to the electron temperature increase, raising the flux of methane, based on the plasma diagnosis results by optical emission spectra (OES). The results of Raman spectroscopy and the X-ray rocking-curve indicated that as-deposited diamonds are of good quality.

**Keywords:** dual radio frequency; inductive coupled plasma jet; single crystal diamond; chemical vapor deposition (CVD); methane flux; growth rate

## 1. Introduction

Diamonds have a large range of potential applications [1–5]. Due to their high atomic density, strong bonding, and crystal structure of high symmetry, diamonds show high Raman gain coefficient, which makes them suitable for high power diamond Raman lasers [6]. With a wide bandgap of 5.5 eV, a high breakdown field, high carrier mobility, and high radiation hardness, diamonds are an ideal material for high energy particle and ionizing radiation detection [7–10]. Furthermore, diamonds exhibit exceptional electronic properties, such as a high breakdown field ( $>10\text{ MV}/\text{cm}$ ) and high carrier mobility ( $4500\text{ cm}^2/\text{Vs}$  for electrons and  $3800\text{ cm}^2/\text{V}$  for holes), which makes diamond an excellent candidate for next generation semiconductor materials [11,12].

Due to the fact that high energy plasma can dissociate reaction gas very effectively and can provide high atomic hydrogen concentration, which is necessary for fabricating high-quality, large area single crystal diamond (SCD), plasma enhanced chemical vapor deposition (PECVD) has been widely used for SCD growth [13]. According to plasma sources, PECVDs can be classified as microwave-, direct current (DC)-, and radio frequency (RF) plasma CVD. Among all these methods, microwave plasma CVD is the most widely used method, the reported largest area reached 2 inches in diameter, and the fastest growth rate reached  $105\text{ }\mu\text{m}/\text{h}$  [14–17].

Like microwave plasma, RF plasma is free from metal electrode contamination. However, RF plasma possess longer wavelengths, so that electrons and positive charged particles in the plasma can get energy from the whole electromagnetic wave vibration period, which leads to more uniform spatial distribution [18]. According to previous reports, plasma density higher than  $10^{18}\text{ m}^{-3}$  can be achieved by radio frequency inductively coupled plasma (RF-ICP). Since the 1980s, researchers have been growing diamond films by RF CVD, and the reported diamond films can be deposited uniformly on a substrate as large as 100 mm in diameter, and the growth rate can reach  $30\text{ }\mu\text{m}/\text{h}$  [19,20]. At the

beginning of the 21st century, the growth rate reached  $70 \mu\text{m/h}$  [21]. However, some drawbacks exist in the RF plasma CVD growth method, such as “hollow shaped” plasma found in the annular discharge zone caused by skin effect easily, which results in a non-diamond composition, and “ion bombardment” caused by plasma self-bias voltage, which damages diamond growth [22,23]. According to our past research, dual RF-ICP can be considered as an effective way to avoid these problems. Moreover, poly-crystal and single-crystal diamond films have been fabricated successfully by very low growth rates [24–27]. In this work, by adjusting growth condition, the growth rate of the SCD films have been greatly enhanced, and the maximum growth rate can exceed  $18 \mu\text{m/h}$ .

## 2. Materials and Methods

Single crystal HPHT Ib (100) diamonds ( $5 \text{ mm} \times 5 \text{ mm}$  and  $6 \text{ mm} \times 6 \text{ mm}$ ) were used as seed substrates. A diagram of the dual RF-ICP jet CVD system used in this work is shown in Figure 1, in which commercial 13.56 MHz and 4 MHz RF power coils were tandemly set on the plasma generator. The high frequency coils were used to excite plasma, and the low frequency coils were used to increase plasma energy. Based on this arrangement, the plasma generator, as well as the reactive gas inlet, were further optimized to increase the SCD deposition rate. A mixture of Ar/H<sub>2</sub>/CH<sub>4</sub> was used as working feed gas with flow rate controlled by the mass-flow controllers. Before deposition process, the substrate was heated to  $300 \text{ }^\circ\text{C}$  in an acid mixture (H<sub>2</sub>SO<sub>4</sub>:HNO<sub>3</sub> = 5:1) for 30 min, followed by ultrasonic clean up under acetone, ethanol, and deionized water to remove excess solvent residues. Detailed deposition parameters are listed in Table 1.

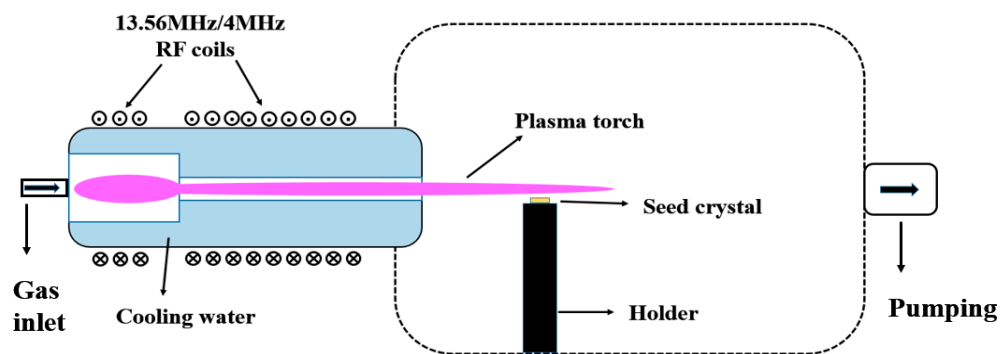


**Figure 1.** A diagram of the dual radio frequency inductively coupled plasma (RF-ICP) jet chemical vapor deposition (CVD) system used in this work.

**Table 1.** Deposition parameters.

Parameters	Value
The gas flow of Ar/H <sub>2</sub> /CH <sub>4</sub>	3.6 slm/1.2 slm/0.04–0.096 slm
Temperature	$800 \text{ }^\circ\text{C} \pm 25 \text{ }^\circ\text{C}$
Chamber pressure	$(8 \pm 0.2) \text{ kPa}$
Plasma power	1 kW(HF) + 9 kW(LF)

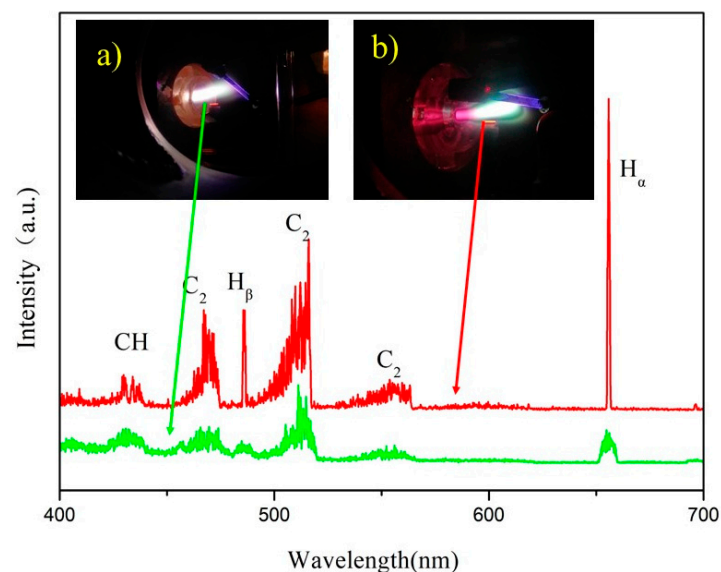
The gas phase species in dual-RF plasma WERE diagnosed by optical emission spectra (OES) (sofn instruments, Beijing, China). The deposited SCDs were characterized by X-ray diffraction (XRD) (Rigaku Ultima IV, Tokyo, Japan), field emission scanning electron microscopy (SEM) (KYKY Technology, Beijing, China) and Raman spectroscopy (Renishaw, London, England).

### 3. Results and Discussion

#### 3.1. Plasma Diagnosed by Optical Emission Spectra (OES)

OES was applied to diagnose the dual-RF plasma, with the working feed gas of Ar/H<sub>2</sub>/CH<sub>4</sub>. OES of plasma was collected through a quartz window under the same instrument parameter setting. The scan range was from 400 nm to 700 nm with a 0.2 nm scanning step.

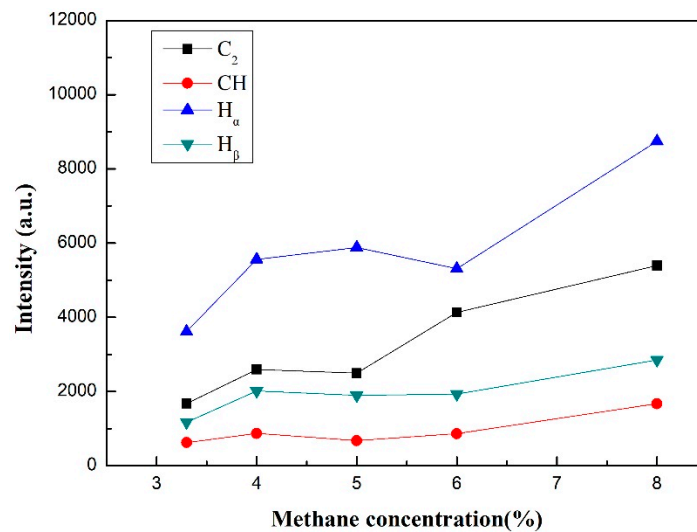
Two introduction methods of feed gas were compared. One was the regular feed gas introduction method, which was used to introduce the mixture of CH<sub>4</sub>/H<sub>2</sub>/Ar to pass through the RF electromagnetic field. The other method was the modified method which was used to introduce the mixture of H<sub>2</sub>/Ar to pass through the RF electromagnetic field, form high density H<sub>2</sub>/Ar plasma beam, and introduce the CH<sub>4</sub> downstream of the H<sub>2</sub>/Ar. This means that the methane was dissociated by H<sub>2</sub>/Ar plasma rather than the RF electromagnetic. Figure 2 is the OES result under the different feed gas introduction methods. The insets are the images of the corresponding plasma. The observed emission peaks correspond to C<sub>2</sub> (471 nm, 516.1 nm, 561 nm swan bands), H<sub>α</sub> (656.1 nm), H<sub>β</sub> (486.1 nm) and CH (388.9 nm and 431.5 nm) for both gas introduction methods, which is a typical spectrum for diamond deposition, just like that of microwave plasma and DC-arc plasma [28,29]. However, the intensity of C<sub>2</sub> and H<sub>α</sub> were higher in the modified method than those in the regular method, which means that the concentration of the H-related radicals and the C-related radicals were higher in case of modified feed gas introduction method. From the insets, it can be seen that the plasma volume in the modified method was larger than that in the regular method, which is suitable for large area diamond deposition. As the quality and growth rate of the deposited diamond films depend on active radical densities on the substrate surface, the modified feed gas introduction method was adopted in the following deposition procedures.



**Figure 2.** Optical emission spectra and plasma torches under two process conditions: (a) old process conditions, (b) improved process conditions.

Figure 3 shows the OES results of the dual-RF plasma. With the methane concentration varying from 3.3% to 8%, the intensity of the C<sub>2</sub> (516.1 nm), H<sub>α</sub> (656.1 nm), H<sub>β</sub> (486.1 nm), CH (431.5 nm) under different CH<sub>4</sub> concentration is plotted in Figure 3. As shown in Figure 3, a slight increase of CH<sub>4</sub> concentration led to a strong increase of both C and H related radicals. This phenomenon is due to the CH<sub>4</sub> dissociation reaction. The change of H<sub>α</sub>, H<sub>β</sub>, and CH intensity was negligible when CH<sub>4</sub> concentration increased from 4% to 6%, however, there was a noticeable increase when CH<sub>4</sub> concentration was higher than 6%. C<sub>2</sub> intensity showed a rapid growth when CH<sub>4</sub> concentration reached 5%. The condition of the plasma can be deduced from the ratio between H<sub>β</sub> and H<sub>α</sub>.

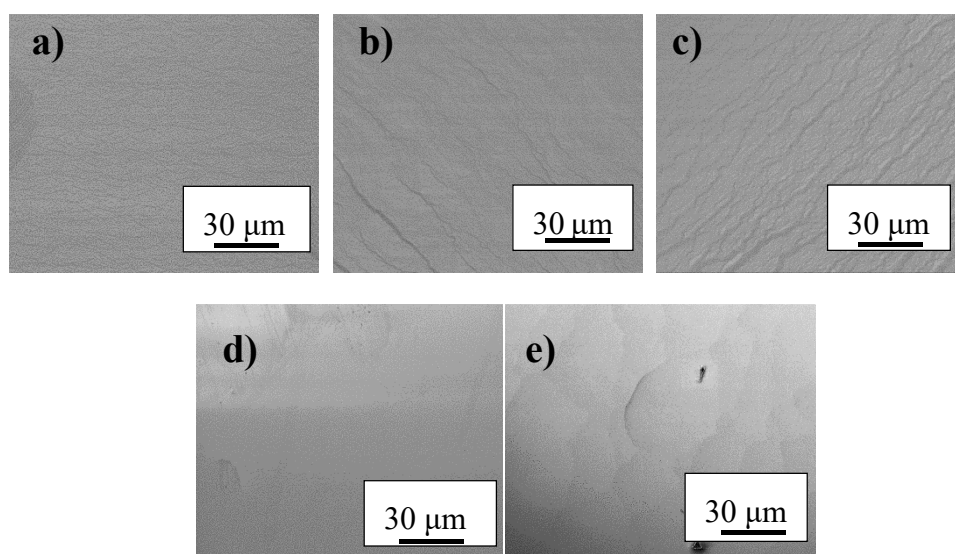
Compared to our previous work [27], the electron temperature ( $T_e$ ) of the plasma was increased from 2.48 eV to 3.92 eV, indicating a strong enhancement of the plasma energy.



**Figure 3.** The emission intensity of the C<sub>2</sub> (516.1 nm), H<sub>α</sub> (656.1 nm), H<sub>β</sub> (486.1 nm), CH (431.5 nm) with methane concentration varying from 3.3% to 8%.

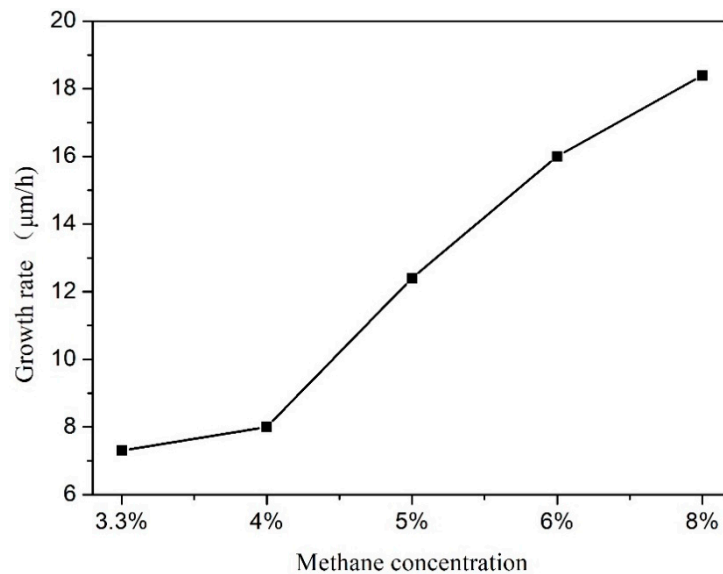
### 3.2. Characterization of Diamond Films

Figure 4 shows the effect of methane concentration on the surface morphology of the deposited diamond films. With the increase of methane concentration, the morphology of the as-grown diamond film changed from stepped growth mechanism to overlapping “hills”, which means that the growth mode changed from 2D layer growth to 3D island growth [30]. From Figure 4a–c, we can see that the diamond film surface was covered by step flows, and with the increase of methane concentration the steps become denser and more disordered. When the methane concentration reached 6%, smooth growth surface was achieved. With further increases of methane concentration, overlapping “hills” can be observed, the growth mechanism changed to island growth, which means that the crystal quality was decreased [31].



**Figure 4.** Surface morphology of the deposited diamond films. the methane concentration: (a) 3.3%; (b) 4%; (c) 5%; (d) 6% and (e) 8%.

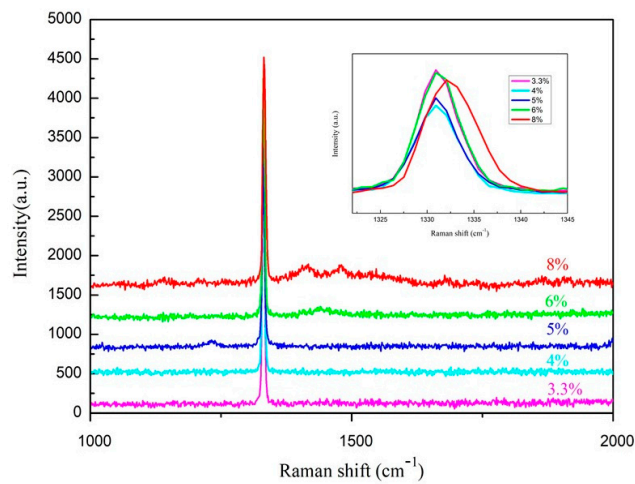
The film deposition rate with different methane concentration is plotted in Figure 5. The deposition rate increased rapidly with the increase of methane concentration. After 10 h deposition, the thickness of the samples increased by 73  $\mu\text{m}$ , 80  $\mu\text{m}$ , 125  $\mu\text{m}$ , 161  $\mu\text{m}$ , and 185  $\mu\text{m}$ , respectively.



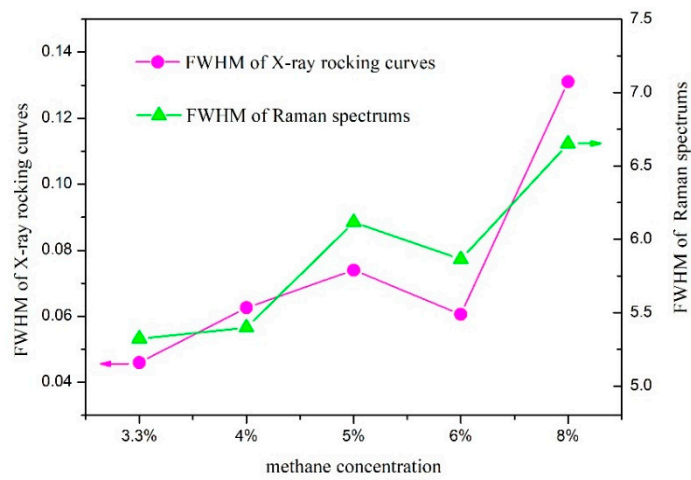
**Figure 5.** Growth rates of the deposited diamond films, with the methane concentration varying from 3.3% to 8%.

Figure 6 shows the Raman spectra of the diamond films. When methane concentration increased from 3.3% to 8%, the diamond peaks were  $1330.8\text{ cm}^{-1}$ ,  $1330.9\text{ cm}^{-1}$ ,  $1330.9\text{ cm}^{-1}$ ,  $1330.9\text{ cm}^{-1}$  and  $1332.1\text{ cm}^{-1}$ , respectively. The position of the diamond peak shows obvious negative shift, indicating a certain amount of tensile stress existed inside the films. According to Boppart's study [32], we can figure out that the specific value of tensile stress was 0.592 GPa, 0.557 GPa, 0.557 GPa, 0.557 GPa and 0.139 GPa, respectively. The tensile stress in the diamond films decreased quickly when methane concentration was higher than 6%. Compared with the surface morphology, when the methane concentration reached 6%, the growth mechanism changed from 2D layer growth to 3D island growth. We guess that the change of growth mechanism led to the reduction of stress in the crystals. From the Raman spectra, we can see that, when the methane concentration was higher than 6%, the scattering broadband among  $1350.0\text{--}1600.0\text{ cm}^{-1}$  was observed, which came from the  $\text{sp}^2\text{ C-C}$  bond. Figure 7 shows the full wave at half maximum (FWHMs) of X-ray rocking curves and Raman spectrums of the deposited diamond films with methane concentration varying from 3.3% to 8%. When the concentration of methane increased, the quality of the SCD films displayed a decreased trend.

When the methane concentration reached 6%, the deposited films showed a relatively high growth rate and good crystal quality. We tried a 50 h deposition at two  $6 \times 6\text{ mm}^2$  HPHT seeds at the same time. The fourier transform infrared spectroscopy (FTIR) of the detached grown layer and HPHT diamond substrate are shown in Figure 8. The inset is the image of the grown diamond. The transmission coefficient of the deposited film was better than the HPHT diamond substrate. At  $1130\text{ cm}^{-1}$ ,  $1282\text{ cm}^{-1}$ , and  $1344\text{ cm}^{-1}$ , deposited diamond film showed lower absorption coefficient, indicating lower nitrogen impurity. The strong bands at  $1900\text{ to }2300\text{ cm}^{-1}$  were the inherent two phonon lines of diamond associated with C–C bonds and were present in both deposited diamond films and HPHT substrates [33]. Figure 9 is the high resolution transmission electron microscopy (HRTEM) micrograph of the deposited single crystal diamond and d-spacing of the deposited diamond was measured to be 0.206 nm, coinciding with that of the diamond (111) plane. There were no defects observed, like dislocations and stacking faults, in the detected zone.



**Figure 6.** Raman spectra of as-grown diamond films when methane concentration varying from 3.3% to 8%.



**Figure 7.** The FWHMs of X-ray rocking curves and Raman spectra of as-grown diamond films with methane concentration varying from 3.3% to 8%.

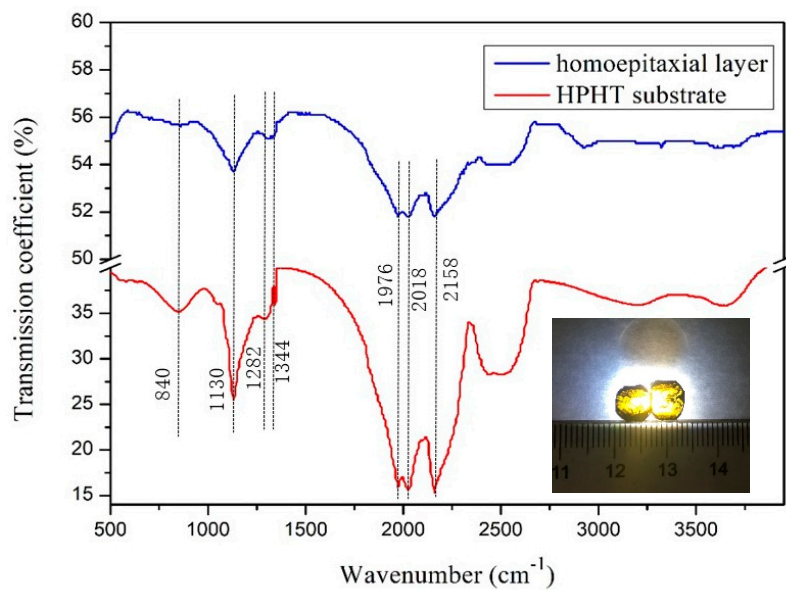


**Figure 8.** FTIR of the deposited CVD film and HPHT diamond substrate.

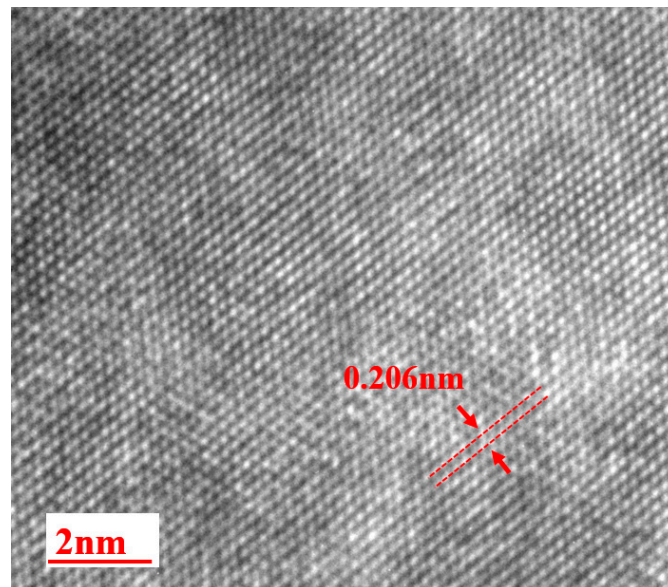


**Figure 9.** HRTEM micrograph of the deposited single crystal diamond.

#### 4. Conclusions

In this article, we investigated single-crystal diamond growth by dual RF-plasma jet CVD. Methane concentration strongly influenced the concentrations of CH, C<sub>2</sub>, H<sub>β</sub>, H<sub>α</sub>, and their proportions in the gas phase, especially C<sub>2</sub>. The morphology of the as-grown diamond film changed from step flows to islands, which means that the growth mode changed from 2D layer growth to 3D island growth. The SCD films were rapidly deposited by dual RF CVD, and the growth rate increased with methane concentration. To our knowledge, this was the first time the fast deposition of single crystal diamond by RF plasma CVD has been realized.

**Author Contributions:** Conceptualization, G.-c.C. and H.L.; methodology, H.L. and J.-j.L.; software, Z.-r.L. and K.X.; validation, H.L., Z.-r.L. and K.X.; formal analysis, H.L.; investigation, Z.-j.C.; resources, Z.-j.C.; data curation, H.L.; writing—original draft preparation, H.L.; writing—review and editing, G.-c.C. and H.L.; supervision, G.-c.C.; project administration, G.-c.C.; funding acquisition, G.-c.C.

**Funding:** This work is supported by National Natural Science Foundation of China (50128790), Hundred program of Chinese Academy of Sciences, Hundred Talents Program of the Chinese Academy of Sciences, Scientific Research Equipment Project of the Chinese Academy of Sciences (yz201356), Hebei Science and Technology Plan (14291110D), Beijing Science and Technology Project (Z151100003315024).

**Conflicts of Interest:** The authors declare no conflict of interest.

#### References

1. May, P.W. The new diamond age. *Science* **2008**, *320*, 1490–1491. [[CrossRef](#)]
2. Isberg, J.; Hammersberg, J.; Johansson, E.; Wikström, T.; Twitchen, D.J.; Whitehead, A.J.; Coe, S.E.; Scarsbrook, G.A. High carrier mobility in single-crystal plasma-deposited diamond. *Science* **2002**, *297*, 1670–1672. [[CrossRef](#)]
3. May, P.W. Diamond thin films: A 21st-century material. *Philos. Trans. R. Soc. Lond. A Math. Phys. Eng. Sci.* **2000**, *358*, 473–495. [[CrossRef](#)]
4. Isberg, J.; Hammersberg, J.; Twitchen, D.J.; Whitehead, A.J. Single crystal diamond for electronic applications. *Diamond Relat. Mater.* **2004**, *13*, 320–324. [[CrossRef](#)]
5. Aharonovich, I.; Castelletto, S.; Simpson, D.A.; Su, C.H.; Greentree, A.D.; Prawer, S. Diamond-based single-photon emitters. *Rep. Prog. Phys.* **2011**, *74*, 076501. [[CrossRef](#)]
6. Williams, R.J.; Kitzler, O.; Bai, Z.; Sarang, S.; Jasbeer, H.; McKay, A.; Mildren, R.P. High Power Diamond Raman Lasers. *IEEE J. Sel. Top. Quantum Electron.* **2018**, *24*, 1–14. [[CrossRef](#)]

7. Obratsova, O.; Ottaviani, L.; Klix, A.; Döring, T.; Palais, O.; Lyoussi, A. Comparing the Response of a SiC and a sCVD Diamond Detectors to 14-MeV Neutron Radiation. *IEEE Trans. Nucl. Sci.* **2018**, *65*, 2380–2384. [[CrossRef](#)]
8. Kumar, A.; Topkar, A. A Study of the Fast Neutron Response of a Single-Crystal Diamond Detector at High Temperatures. *IEEE Trans. Nuclear Sci.* **2018**, *65*, 630–635. [[CrossRef](#)]
9. Girolami, M.; Bellucci, A.; Calvani, P.; Trucchi, D.M. Large single-crystal diamond substrates for ionizing radiation detection. *Phys. Status Solidi A* **2016**, *213*, 2634–2640. [[CrossRef](#)]
10. Schirru, F.; Kisielewicz, K.; Nowak, T.; Marczevska, B. Single crystal diamond detector for radiotherapy. *J. Phys. D Appl. Phys.* **2010**, *43*, 265101. [[CrossRef](#)]
11. Umezawa, H. Recent advances in diamond power semiconductor devices. *Mater. Sci. Semicond. Process.* **2018**, *78*, 147–156. [[CrossRef](#)]
12. Yamaguchi, H.; Masuzawa, T.; Nozue, S.; Kudo, Y.; Saito, I.; Koe, J.; Okano, K. Electron emission from conduction band of diamond with negative electron affinity. *Phys. Rev. B* **2009**, *80*, 165321. [[CrossRef](#)]
13. Silva, F.; Achard, J.; Brinza, O.; Bonnin, X.; Hassouni, K.; Anthonis, A.; Barjon, J. High quality, large surface area, homoepitaxial MPACVD diamond growth. *Diamond Relat. Mater.* **2009**, *18*, 683–697. [[CrossRef](#)]
14. Ralchenko, V.G.; Smolin, A.A.; Konov, V.I.; Sergeichev, K.F.; Sychov, I.A.; Vlasov, I.I.; Khomich, A.V. Large-area diamond deposition by microwave plasma. *Diamond Relat. Mater.* **1997**, *6*, 417–421. [[CrossRef](#)]
15. Silva, F.; Hassouni, K.; Bonnin, X.; Gicquel, A. Microwave engineering of plasma-assisted CVD reactors for diamond deposition. *J. Phys. Condens. Matter* **2009**, *21*, 364202. [[CrossRef](#)]
16. Yamada, H.; Chayahara, A.; Ohmagari, S.; Mokuno, Y. Factors to control uniformity of single crystal diamond growth by using microwave plasma CVD. *Diamond Relat. Mater.* **2016**, *63*, 17–20. [[CrossRef](#)]
17. Li, F.; Zhang, J.; Wang, X.; Zhang, M.H.; Wang, H.X. Fabrication of Low Dislocation Density, Single-Crystalline Diamond via Two-Step Epitaxial Lateral Overgrowth. *Crystals* **2017**, *7*, 114. [[CrossRef](#)]
18. Kim, Y.D.; Lee, H.C.; Chung, C.W. A study on the maximum power transfer condition in an inductively coupled plasma using transformer circuit model. *Phys. Plasmas* **2013**, *20*, 093508. [[CrossRef](#)]
19. Matsumoto, S.; Hino, M.; Kobayashi, T. Synthesis of diamond films in a rf induction thermal plasma. *Appl. Phys. Lett.* **1987**, *51*, 737–739. [[CrossRef](#)]
20. Kohzaki, M.; Uchida, K.; Higuchi, K.; Noda, S. Large-area high-speed diamond deposition by RF induction thermal plasma chemical vapor deposition method. *Jpn. J. Appl. Phys.* **1993**, *32*, L438. [[CrossRef](#)]
21. Berghaus, J.O.; Meunier, J.L.; François, G. Direct current bias effects in RF induction thermal plasma diamond CVD. *IEEE Trans. Plasma Sci.* **2002**, *30*, 442–449. [[CrossRef](#)]
22. Greenfield, S. Invention of the annular inductively coupled plasma as a spectroscopic source. *J. Chem. Educ.* **2000**, *77*, 584. [[CrossRef](#)]
23. Dayal, S.; Sasikumar, C.; Srivastava, S. Development of ultra-smooth ballas diamond incorporated nano-composite carbon thin films using PECVD technique. *J. Mater. Sci. Mater. Electron.* **2016**, *27*, 8188–8196. [[CrossRef](#)]
24. Shi, Y.C.; Li, J.J.; Liu, H.; Zuo, Y.G.; Bai, Y.; Sun, Z.F.; Ma, D.L.; Chen, G.C. Nano-Crystalline Diamond Films Grown by Radio-Frequency Inductively Coupled Plasma Jet Enhanced Chemical Vapor Deposition. *Chin. Phys. Lett.* **2015**, *32*, 088104. [[CrossRef](#)]
25. Bai, Y.; Zuo, Y.G.; Li, J.J.; Liu, H.; Yuan, H.W.; Chen, G.C. Effect of water-cooling and sheath gas-cooling in a jet driven by RF-ICP studied by means of numerical simulation. *Diamond Relat. Mater.* **2017**, *73*, 72–79. [[CrossRef](#)]
26. Li, J.J.; Li, B.; Zuo, Y.G.; Liu, H.; Bai, Y.; Yuan, H.W.; Li, Z.R.; Xu, K.; Chen, G.C. Application of dual radio frequency inductive coupled plasma into CVD diamond growth. *Vacuum* **2018**, *154*, 174–176. [[CrossRef](#)]
27. Zuo, Y.G.; Li, J.J.; Bai, Y.; Liu, H.; Yuan, H.W.; Chen, G.C. Growth of nanocrystalline diamond by dual radio frequency inductively coupled plasma jet CVD. *Diamond Relat. Mater.* **2017**, *73*, 67–71. [[CrossRef](#)]
28. Ma, J.; Ashfold, M.N.R.; Mankelevich, Y.A. Validating optical emission spectroscopy as a diagnostic of microwave activated CH<sub>4</sub>/Ar/H<sub>2</sub> plasmas used for diamond chemical vapor deposition. *J. Appl. Phys.* **2009**, *105*, 043302. [[CrossRef](#)]
29. Rennick, C.J.; Ma, J.; Henney, J.J.; Wills, J.B.; Ashfold, M.N.R.; Orr-Ewing, A.J.; Mankelevich, Y.A. Measurement and modeling of Ar/H<sub>2</sub>/CH<sub>4</sub> arc jet discharge chemical vapor deposition reactors. I. Intercomparison of derived spatial variations of H atom, C<sub>2</sub>, and CH radical densities. *J. Appl. Phys.* **2007**, *102*, 063309. [[CrossRef](#)]

30. Muehle, M.; Asmussen, J.; Becker, M.F.; Schuelke, T. Extending microwave plasma assisted CVD SCD growth to pressures of 400 Torr. *Diamond Relat. Mater.* **2017**, *79*, 150–163. [[CrossRef](#)]
31. Tokuda, N. Homoepitaxial diamond growth by plasma-enhanced chemical vapor deposition. In *Novel Aspects of Diamond*; Springer: Cham, Switzerland, 2015; pp. 1–29.
32. Boppart, H.; Van Straaten, J.; Silvera, I.F. Raman spectra of diamond at high pressures. *Phys. Rev. B* **1985**, *32*, 1423. [[CrossRef](#)]
33. Anthony, T.R.; Banholzer, W.F. Properties of diamond with varying isotopic composition. *Diamond Relat. Mater.* **1992**, *1*, 717–726. [[CrossRef](#)]



© 2019 by the authors. Licensee MDPI, Basel, Switzerland. This article is an open access article distributed under the terms and conditions of the Creative Commons Attribution (CC BY) license (<http://creativecommons.org/licenses/by/4.0/>).